



# International Journal of Crashworthiness

ISSN: 1358-8265 (Print) 1754-2111 (Online) Journal homepage: <http://www.tandfonline.com/loi/tcrs20>

## Dynamic bending behaviour of magnesium alloy rectangular thin-wall beams filled with polyurethane foam

Ping Zhou, Elmar Beeh, Michael Kriescher, Horst E. Friedrich & Gundolf Kopp

To cite this article: Ping Zhou, Elmar Beeh, Michael Kriescher, Horst E. Friedrich & Gundolf Kopp (2016): Dynamic bending behaviour of magnesium alloy rectangular thin-wall beams filled with polyurethane foam, International Journal of Crashworthiness, DOI: [10.1080/13588265.2016.1208715](https://doi.org/10.1080/13588265.2016.1208715)

To link to this article: <http://dx.doi.org/10.1080/13588265.2016.1208715>



Published online: 22 Jul 2016.



Submit your article to this journal [↗](#)



Article views: 12




View related articles [↗](#)



View Crossmark data [↗](#)

Full Terms & Conditions of access and use can be found at  
<http://www.tandfonline.com/action/journalInformation?journalCode=tcrs20>

# Dynamic bending behaviour of magnesium alloy rectangular thin-wall beams filled with polyurethane foam

Ping Zhou , Elmar Beeh, Michael Kriescher, Horst E. Friedrich and Gundolf Kopp

German Aerospace Centre (DLR), Institute of Vehicle Concepts, Stuttgart, Germany

## ABSTRACT

This study proposes a hybrid structural design concept of polyurethane foam-filled magnesium alloy AZ31B rectangular thin-walled beams which serve as energy absorbing components in automotive applications. Uniaxial tensile and compressive tests, and fracture tests were performed to investigate the material mechanical properties. Dynamic three-point bending tests were performed to study the deformation/fracture modes and energy absorption capacity for the foam-filled AZ31B beams, and to compare these mechanical properties with those for mild steel DC04 beams. Different AZ31B beams were filled with a variation of foam density (0.05, 0.20 and 0.30 g/cm<sup>3</sup>). It was found that the AZ31B beam filled with 0.20 g/cm<sup>3</sup> foam reached the highest specific energy absorption; moreover, it absorbed more energy and reached much higher specific energy absorption than the foam-filled DC04 beam filled with the same foam, although the former one was nearly 54% lighter. The potential advantage of the foam-filled AZ31B beams is possibly associated with the high work hardening rate of AZ31B sheet in compression, which may involve more material in plastic deformation compared with the foam-filled DC04 beams. It has therefore been demonstrated that the hybrid structural design concept of the polyurethane foam-filled AZ31B beam has potential applications in auto-body structures.

## ARTICLE HISTORY

Received 5 August 2015  
Accepted 28 June 2016

## KEYWORDS

Magnesium alloy; polyurethane foam; thin-walled structure; hybrid structure; energy absorption; fracture behaviour

## 1. Introduction

Magnesium alloys, such as the lowest density structural metals, have always been attractive to automotive manufacturers due to their inherent advantages such as low density ( $\approx 1.8$  g/cm<sup>3</sup>), high strength-to-weight ratio, high damping resistance and easy recycling, which make them provide an effective way to achieve weight reduction. High-pressure die casting (HPDC) products, such as engine components, transmission cases, steering wheels and instrument panels, have been applied in some high-class and luxury cars [17,18,21]. For many applications in the automotive industry, the crashworthiness of a structure is an important property which must be addressed by design engineers. In recent years, the European collaborative R&D project 'SuperLIGHT-CAR' [5,24] and the Canada–China–USA collaborative R&D project 'MFERD' [20] carried out a large amount of systematic research to apply HPDC magnesium parts in crash-related vehicle structures. One of the challenging tasks is to develop technical strategies which can control the deformation and failure of HPDC magnesium parts because they tend to fracture prematurely under crash loads [5]. In order to increase the use of magnesium alloys and make a constant weight

reduction, more attention has been paid to employing wrought magnesium alloys as crashworthy components in auto-body structures, because wrought magnesium alloys exhibit higher strength and greater ductility than HPDC magnesium alloys.

Magnesium alloys have a hexagonal close-packed (HCP) structure and can only initiate limited slip and twinning systems at room temperature, which results in lower ductility than some steels and aluminium alloys [34]. Moreover, the c-axis of HCP structure generally aligns perpendicular to the rolling and extrusion direction during traditional rolling and extrusion processes, respectively, which leads to strong plastic anisotropy [22,29,33,35] and tension-compression asymmetry [32,34,35]. Therefore, wrought magnesium alloys exhibit inferior room temperature ductility and formability which limit their crashworthiness applications in automotive industry. In forming applications, these issues can be overcome by increasing the forming temperature because more deformation mechanisms can be activated [35]. Another predominant feature of wrought magnesium alloys is the strain rate sensitivity in tension and compression [32,33,42,46], which offers an advantage in energy absorption (EA) in crash scenarios.

In the past two decades, a number of researchers [7,14,15,26,39,40,47] carried out extensive studies on the bending behaviour of steel and aluminium thin-walled beams filled with lightweight foams by using experimental, analytical and numerical methods. It was found that the internal lightweight foam filler is able to stabilise the cross-section of thin-walled beam and retards the local sectional collapse at the compression wall, and therefore significantly improves the load carrying capacity and specific energy absorption. However, relatively little research has been done in examining the crashworthiness and deformation modes include fracture modes of magnesium alloy thin-walled structures subjected to bending loads, although some investigations [6,9–12,37,38,41,43,44] have been focused on the deformation behaviour under axial compressive loads in recent two decades.

Dørum et al. [9,10] studied the bending resistance and fracture behaviour of HPDC magnesium AM60 U-shaped thin-walled beams and found that the material's inhomogeneous micro-mechanical properties in uniaxial tension and initial geometric imperfections of the profiles lead to a large scatter on the mechanical response of the beams. Easton et al. [19] investigated the EA capacity of several HPDC magnesium alloys and wrought magnesium alloy AZ31, and compared them with mild steel HA300 and aluminium alloy 6061-T6 plates in bending and buckling. The experimental investigation performed by Hilditch et al. [27] demonstrated that the magnesium alloy AZ31 extruded circular tube in three-point bending has higher load carrying capacity and EA performance than an equivalent mass tube made of aluminium alloy with similar tensile yield strength. Wagner et al. [44] and Ali [1] studied the bending collapse and its numerical simulation method of thin-walled rectangular magnesium alloy AZ31 sheet beams. Based on these investigations, it comes out that some HPDC

magnesium alloys and wrought alloy AZ31 thin-walled beams in bending and buckling significantly outperform steels and aluminium alloys with respect to specific energy absorption. This outperformance may be due to the following two inherent features. First, magnesium thin-walled beam has higher moment of inertia due to the thicker cross-section which is achieved by its lower density while maintaining its mass. Second, probably due to the significantly higher work hardening rate in compression, magnesium thin-walled beam shows a larger radius of curvature, and therefore more material is involved in plastic deformation. Nevertheless, magnesium thin-walled beam is susceptible to fracture at plastic hinges at a relatively small rotation, which results in rapidly drop of bending resistance.

Structural polyurethane (PUR) foams, as a kind of cellular materials, have attracted increasing attention as filler materials for empty thin-walled structures, owing to their excellent EA and stiffness performance [23]. Moreover, they provide multi-functional benefits such as weight reduction potential, design flexibility and scalability. Therefore, they have been widely used in automotive industry to prevent occupant injuries in vehicle crash scenarios. As shown in Figure 1, typical applications include cross beams, A–D pillars, roof joints, rocker rails, door frames, bumper system, and so on. As reported in [3,36], the stress–strain curve of a PUR foam in uniaxial compression can be characterised by three sequential phases: linear elasticity, plateau stress and densification. It can not only undergo large compressive deformation and thus absorb a considerable amount of energy through cell bending, buckling or fracture, but also maintain an almost constant stress during the plateau stress phase, which is an excellent characteristic of EA in automotive applications. Moreover, PUR foams exhibit considerable strain rate sensitivity as reported in [3,8,28].

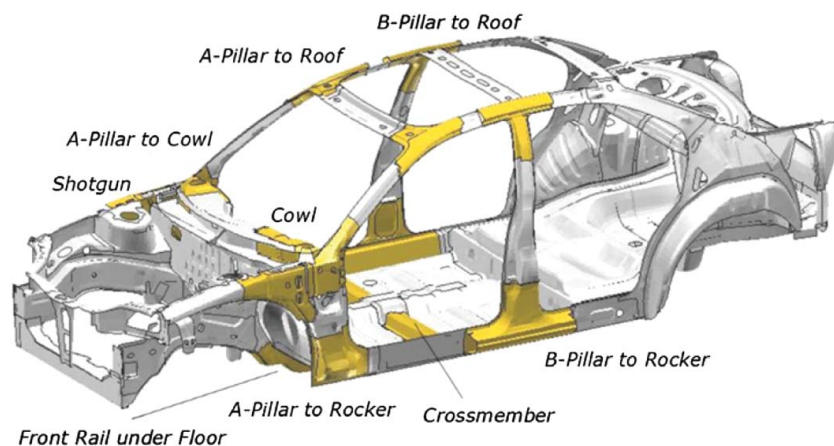


Figure 1. Typical applications of structural polyurethane foams in auto-body structures [13].

This study proposes a hybrid structural design concept, in which magnesium alloy AZ31B rectangular thin-walled beams are filled with PUR foams and serve as energy absorbing components in automotive applications. The main purpose of this study is three-fold. First, the principle mechanical properties of AZ31B and PUR foam, such as strength and ductility, are studied at a macro-level by quasi-static uniaxial tensile and compressive tests. Second, dynamic bending collapse behaviour of empty and PUR foam-filled AZ31B rectangular thin-walled beams, such as force–deflection curve characteristics, deformation modes, fracture modes and EA capacity, are investigated experimentally and compared with the results from the mild steel DC04 thin-walled beams, which were previously studied by two of current authors [30]. Third, potential applications of the hybrid structural design concept of PUR foam-filled AZ31B beams are discussed. Different foam-filled magnesium beams with a variation of foam density were fabricated through several manufacturing processes: cold bending, tungsten inert gas welding, cathodic dip painting and polyurethane foam injection. It should be noted that this paper does not aim to compressively study the influences of manufacturing processes (cold bending, tungsten inert gas welding and cathodic dip painting), nor does it aim to thoroughly investigate the effect of foam density on the mechanical properties discussed. Therefore, only three different levels of foam density (0.05, 0.20 and 0.30 g/cm<sup>3</sup>) are preliminarily examined in present experimental work. To our knowledge, this is the first experimental demonstration of PUR foam-filled magnesium thin-walled structures subjected to dynamic bending loads.

## 2. Materials and experiments

### 2.1. Materials

Empty and PUR foam-filled rectangular thin-walled beams were investigated in this study. The beam shells were made of magnesium alloy AZ31B (Mg-3Al-1Zn-0.3Mn, wt. %) in the form of fully annealed (O-temper) sheet. The sheets with a nominal thickness of 1.8 mm were fabricated by twin-roll cast and rolled processes in ThyssenKrupp MgF Magnesium Flachprodukte GmbH. The average grain size is about 13 μm as can be seen from the microstructure of the as-received AZ31B sheets in Figure 2. For comparison purpose, a cold rolled mild steel DC04 with a nominal thickness of 2.0 mm was chosen on the basis of two considerations: the relatively widespread use of this steel in auto-body structures and availability of our previously published experimental results [30] obtained to allow for comparisons.

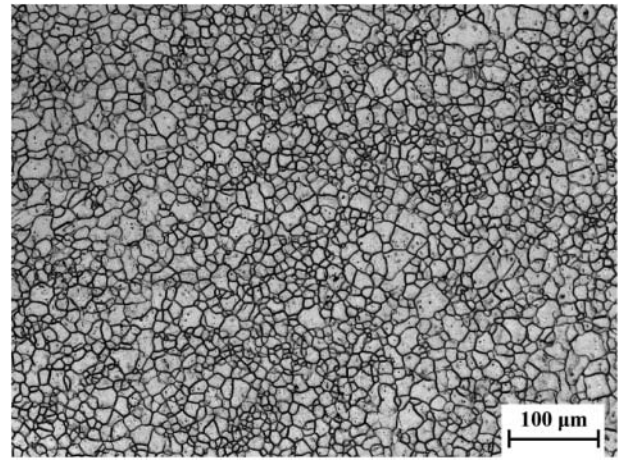


Figure 2. Microstructure of the as-received AZ31B sheets.

Two types of closed-cell rigid PUR foams were chosen as filler materials: (i) PUR pre-polymer building foam with a nominal density of 0.05 g/cm<sup>3</sup> and (ii) BETAFOAM™ PUR structural foam with three different nominal densities (0.20, 0.30 and 0.40 g/cm<sup>3</sup>) which were produced by The Dow Chemical Company.

### 2.2. Uniaxial tensile and compressive tests

To examine the mechanical properties of AZ31B sheet and PUR foams in uniaxial tensile and compressive loads at room temperature, a static universal material testing machine Zwick Roell Z250 was employed to conduct the uniaxial tensile and compressive tests at the German Aerospace Centre (DLR) – Institute of Vehicle Concepts in Stuttgart. The quasi-static tensile tests for AZ31B sheet were carried out in accordance with standard ASTM E8 at a crosshead velocity of 2.1 mm/min, while the uniaxial compressive tests for AZ31B sheet were carried out by using a newly developed testing method [48]. For the PUR foams, the uniaxial tensile or compressive tests were conducted by the material supplier. The PUR foams were tested by quasi-statically compressing or pulling a cubic specimen with dimensions 50 × 50 × 50 mm along one direction.

### 2.3. Fracture tests at different stress states

Generally, macro-fracture strain is a quantitative measure of ductility for metals. In recent years, it has been reported that the fracture strain depends on the material stress state which is represented by the stress triaxiality and Lode parameter [4,16,25,45]. The stress state is represented by the stress triaxiality which is defined as the

ratio of hydrostatic stress and von Mises stress. In order to study the fracture characteristics of AZ31B sheet, different shapes of thin-sheet specimens were tested under quasi-static loading conditions using the static universal material testing machine Zwick Roell Z250. The specimen geometries were designed to vary the stress states such as uniaxial compression, pure shear, uniaxial tension and plane strain conditions. ARAMIS Digital Image Correlation system (GOM GmbH, Germany) was used to measure the localised effective failure strain. For more details about the specimen geometries and experimental procedures, the readers can refer to the research done by Gruben et al. [25].

## 2.4. Three-point bending tests

### 2.4.1. Specimens

The empty and foam-filled steel and magnesium rectangular thin-walled beams, as a simplified full-scale component of a typical auto-body structure, i.e. a rocker rail as shown in Figure 3(a), were constructed using simplified geometric dimensions. The cross-sections of different simplified structures are shown in Figure 3(b)–(e). All the beams have the same total length of 2000 mm. Two different corner types using chamfers and fillets were designed for the steel and magnesium beams, respectively. Chamfered corners were designed for the

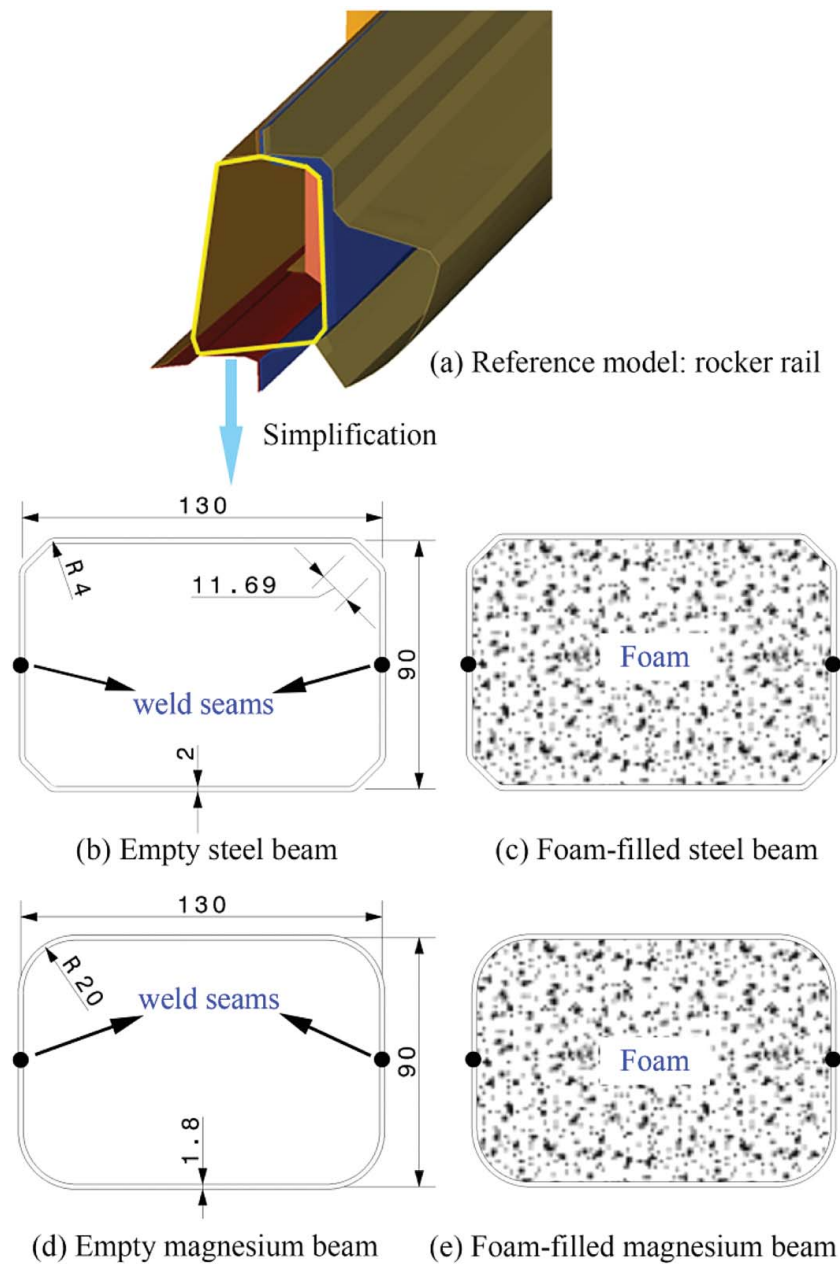


**Figure 3.** Cross-sections of empty/foam-filled steel and magnesium beams. Note: All dimensions are in millimetres.

steel beams, while filleted corners for the magnesium beams to prevent pre-damage during cold bending. The beams were produced by several manufacturing processes. First, the sheets were trimmed and bent into U-shaped profiles at room temperature. Next, two U-shaped profiles were joined along the two flanges by resistance seam welding and tungsten inert gas welding for the steel and magnesium beams, respectively. Then, the beams were treated by cathodic dip painting to guarantee a good interface connection between the metallic shell and foam filler. Finally, the beam cavities were fully filled with PUR foams.

It is well-known that the corner type of thin-walled beams may affect the mechanical behaviour in some applications. Therefore, the effect of the corner type on the mechanical behaviour of the studied beams in bending collapse will be discussed. The manufacturing processes such as the cold bending, tungsten inert gas welding and cathodic dip painting were commercially conducted by external manufacturing suppliers and thus the detailed processing parameters are not available for the authors.

#### 2.4.2. Testing setup

The rocker rail is one of the major energy absorbing components in passenger car pole side impact scenarios. Three-point bending tests on the steel and magnesium beams were conducted with the testing parameters which approximate the loading and boundary conditions in NCAP (New Car Assessment Programme) pole side impact tests. Dynamic three-point bending tests on the steel and magnesium beams were performed using the DLR-dynamic component testing system which was constructed in house at the DLR-Institute of Vehicle Concepts in Stuttgart. As shown in Figure 4, the diameters of the cylindrical indenter and two fixed supports

are 300 mm and 96 mm, respectively. The specimens were placed centrally on the two supports with a span length of 1368 mm. The testing system comprised of a pneumatic-cylinder actuator, a moving sled with a minimum mass of 767 kg, a fixed sled, two sliding rails, an accelerometer and three high speed cameras (Photron FASTCAM SA3). The accelerometer was embedded inside the moving sled to record acceleration history which was converted to force signal. The high speed cameras were used to record the deformation, speed and displacement history with a motion analysis programme (TEMA Motion Analysis). To be noted, the minimum impact mass of 767 kg was high for the current tests; therefore compromised lower speeds (2.0 m/s and 3.5 m/s) were chosen to prevent potential risk of fixture damage due to dissipating remaining kinetic energy. The quasi-static three-point bending tests on the empty and foam-filled steel beams, which were previously studied by two of current authors [30], employed a horizontal servo-hydraulic testing machine with an MTS load cell. The quasi-static tests were conducted at a constant speed of 60 mm/s and terminated after reaching a prescribed deflection of 450 mm.

#### 2.4.3. Testing matrix

Four different magnesium beams together with four different steel beams are summarised in Table 1, where the mass represents the total mass of the thin-wall beam and foam filler. For simplicity, the specimens were identified by letters and numbers. The first letter 'S' stands for a steel beam and 'M' for a magnesium beam; the middle letter 'E' stands for empty and middle number denotes the foam density; the last letter 'S' stands for a quasi-static loading condition and 'D' for a dynamic loading condition. Three to five repeat specimens were tested for each testing case.

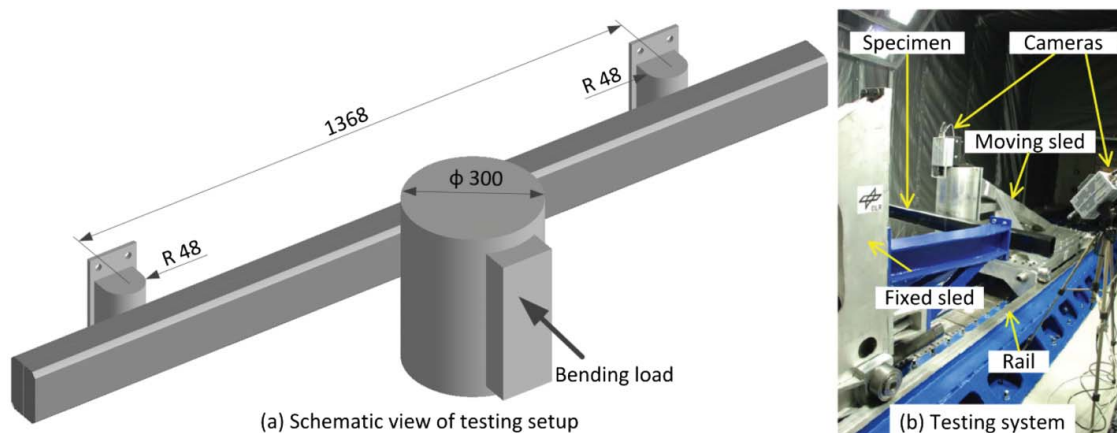


Figure 4. Three-point bending test facility and setup. Note: All dimensions are in millimetres.

**Table 1.** Summary of testing matrix and specimen details.

Specimen	Shell material	Foam	Mass (kg)	Speed (m/s)
Empty and foam-filled steel beams				
SES	Steel DC04	Empty	12.35	0.06
S20S	Steel DC04	0.20 kg/cm <sup>3</sup>	16.92	0.06
S40S	Steel DC04	0.40 kg/cm <sup>3</sup>	21.15	0.06
S40D	Steel DC04	0.40 kg/cm <sup>3</sup>	21.15	6.0
Empty and foam-filled magnesium beams				
MED	Mg AZ31B	Empty	2.73	2.0
M05D	Mg AZ31B	0.05 kg/cm <sup>3</sup>	3.75	2.0
M20D	Mg AZ31B	0.20 kg/cm <sup>3</sup>	7.70	3.5
M30D	Mg AZ31B	0.30 kg/cm <sup>3</sup>	9.58	3.5

### 3. Coupon test results

#### 3.1. Uniaxial mechanical properties

The quasi-static true stress–strain curves in uniaxial tensile and compressive loads for steel DC04 and magnesium AZ31B sheet in the rolling direction (RD), diagonal direction (DD) and transverse direction (TD) at room temperature are shown in Figure 5(a) and 5(b). The results present that AZ31B sheet exhibits moderate anisotropy of yield strength in both tension and compression, but it exhibits relatively significant anisotropy of fracture elongation in tension. Moreover, a pronounced tension-compression asymmetry and very high work hardening rate in compression was observed for AZ31B sheet. Compared with DC04 sheet, AZ31B sheet exhibits slightly lower yield strength; however, it exhibits much lower ultimate tensile strength and ductility.

The typical engineering stress–volumetric strain curves for the PUR foams of three different densities are shown in Figure 5(c). Each curve in uniaxial compression shows a significant plateau stress phase. During this phase the foam undergoes a large compressive deformation and absorbs a considerable amount of energy. In uniaxial tension, however, the brittle fracture occurs at a small strain. It is evident that the flow stress of the PUR foams increases with increasing foam density.

#### 3.2. Fracture characteristics at different stress states

As shown in Figure 6, AZ31B sheet exhibits a significant variation in ductility as a function of the stress triaxiality. The effective failure strain was measured at the region of the localised plastic deformation just before final fracture on each tested specimen. It is evident that the effective failure strain is higher in the uniaxial tension condition, while much lower in the uniaxial compression and plain strain conditions.

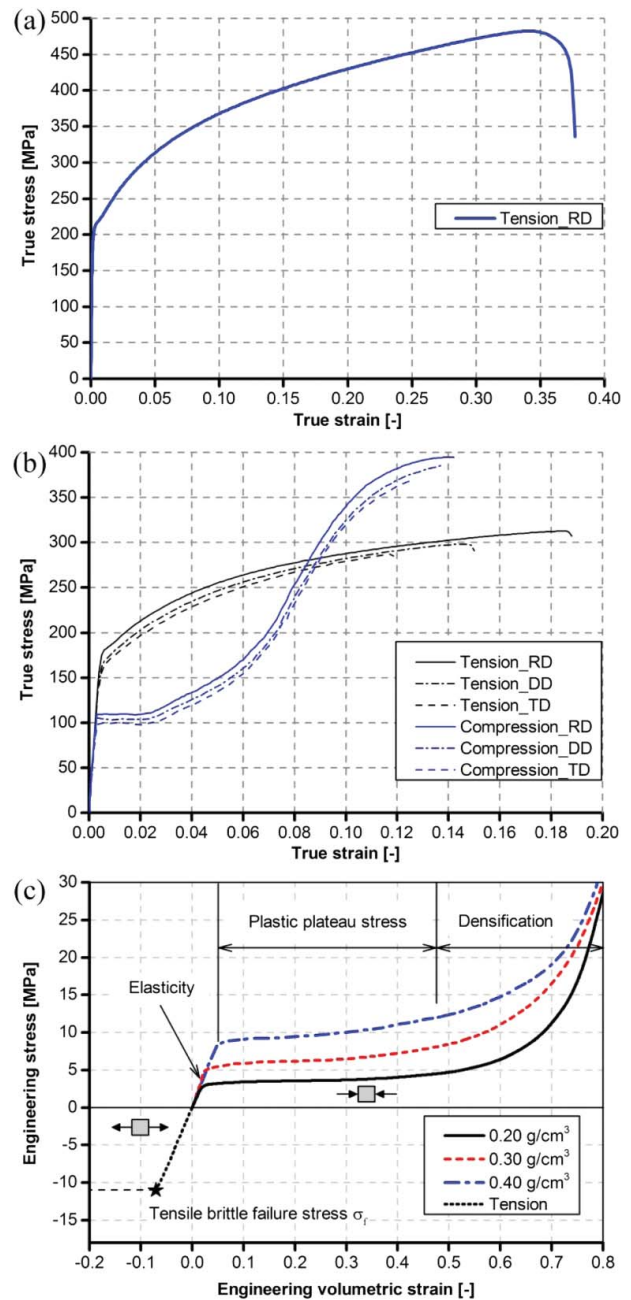


**Figure 5.** (a) Tensile true stress–strain curve for steel DC04, (b) tensile/compressive true stress–strain curves for magnesium alloy AZ31B and (c) typical tensile/compressive engineering stress–volumetric strain curves for polyurethane foams. Note: All curves were obtained at a nominal strain rate of  $0.001\text{s}^{-1}$  and room temperature. RD: rolling direction, DD: diagonal direction, TD: transverse direction.

### 4. Three-point bending test results

The typical experimental results of the empty and foam-filled magnesium beams and a wide range of comparisons with the results of the steel beams are reported in terms of force–deflection curves and deformation/failure modes in the following subsections.

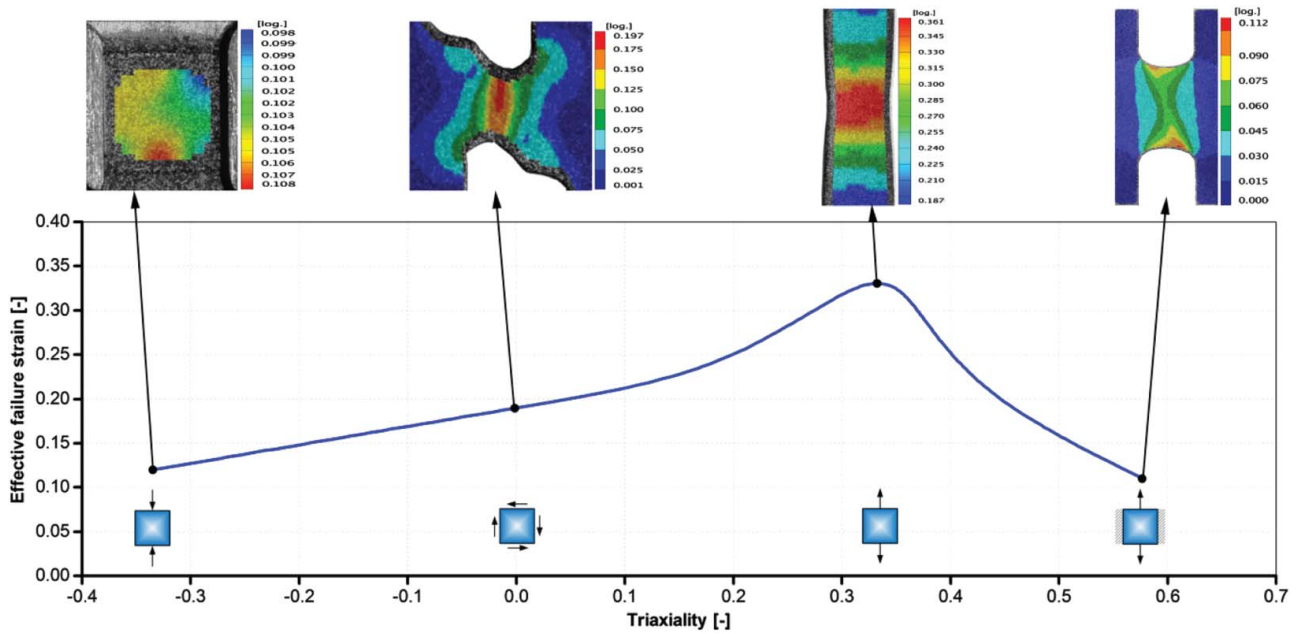


**Figure 6.** Effective failure strain versus average stress triaxiality for AZ31B sheet. Note: The color maps show the distributions of the equivalent strains on the specimens before fracture.

#### 4.1. Force–deflection curves

The intrusion displacement of rocker rails in passenger cars should be generally not larger than 450 mm even in severe crash accidents due to the passenger safety protection according to most passive safety regulations and NCAP side impact tests [2]. Therefore, the mechanical behaviour of the tested beams in the quasi-static and dynamic bending tests was studied only within a deflection of 450 mm.

The typical force–deflection curves of the empty and foam-filled magnesium beams shown in Figure 7(a), while Figure 7(b) shows the corresponding results of the

empty and foam-filled steel beams for comparison purposes. The quantitative analysis of the peak crushing force, maximum deflection, total EA and specific EA for all the structures are summarised in Table 2.

##### 4.1.1. Characterisation of force–deflection curves

It can be seen from Figure 7 that the force–deflection curves have different shapes which are associated with the deformation behaviour of the different structures. The curves of MED and M05D have a similar shape to SES and S20S. They can be characterised by three phases: (i) a linear elasticity; (ii) a slow plasticisation up to the

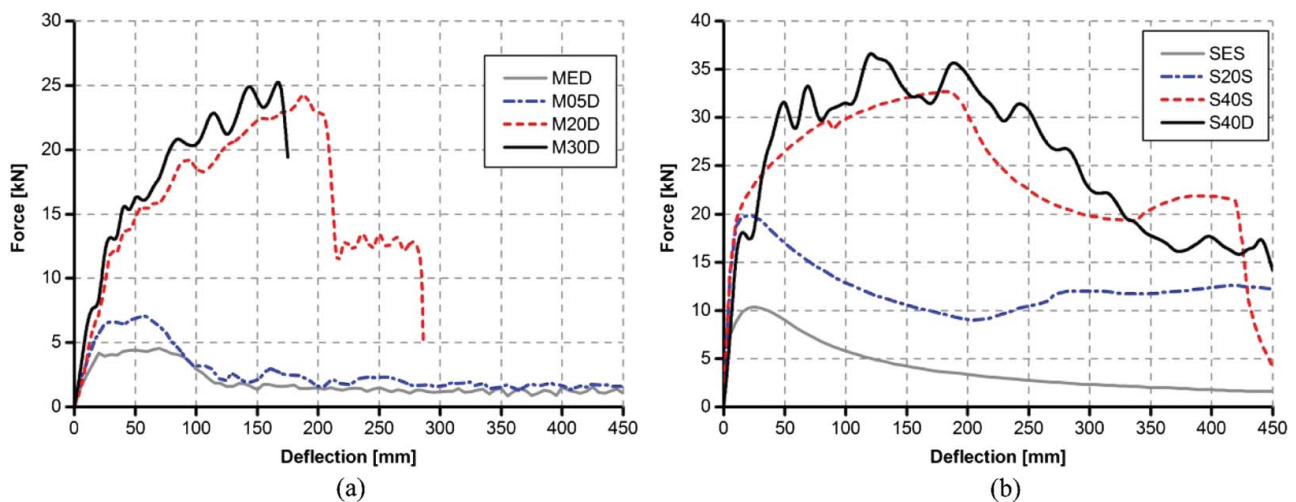


**Figure 7.** Force–deflection curves: (a) magnesium AZ31B beams [30] and (b) steel DC04 beams.



**Table 2.** Summary of testing results for different structures at different deflections.

Specimen	Mass (kg)	Peak force (kN)	Max. deflection (mm)	Energy absorption (kJ)				Specific energy absorption (J/kg)			
				450 mm	350 mm	250 mm	150 mm	450 mm	350 mm	250 mm	150 mm
Empty and foam-filled steel beams											
SES	12.35	10.3	450	1.80	1.64	1.40	1.06	146	133	113	86
S20S	16.92	20.0	450	5.31	4.32	3.16	2.19	314	255	187	129
S40S	21.15	32.7	420	10.78	8.96	6.94	4.05	507	424	327	191
S40D	21.15	34.1	440	11.54	9.87	7.51	4.27	543	467	353	202
Empty and foam-filled magnesium beams											
MED	2.73	4.6	450	0.88	0.75	0.62	0.47	321	275	228	172
M05D	3.75	7.0	450	1.23	1.06	0.88	0.66	329	283	234	176
M20D	7.70	24.3	285	4.71	4.71	4.21	2.29	612	612	546	297
M30D	9.58	24.6	175	3.19	3.19	3.19	2.58	333	333	333	269

Note: The maximum deflection represents the deflection when the beam was thoroughly broken up into two pieces and lost the load carrying capacity. In the case of SES, S20S, MED and M05D, the beams were not thoroughly broken up into two pieces and the maximum deflection represents the maximum considered deflection, i.e. 450 mm in the current study.

The peak force represents the average force of the highest wave in the force–deflection curves for S40D and M30D. For other specimens, the peak force represents the maximum crushing force.

peak crushing force; (iii) a slow load drop. However, the peak crushing force of MED and M05D occur at a larger amount of deflection compared with those of SES and S20S; moreover, the rates of load decreasing after the peak crushing force for MED and M05D are noticeably lower than those for SES and S20S. Therefore, the former ones have ‘invert-U’ shaped curves while the later ones have ‘invert-V’ shaped curves in the vicinity of the peak crushing force. On the other hand, the curve of M20D shows a different shape compared with S20S, although both M20D and S20S were filled with 0.20 g/cm<sup>3</sup> PUR foam. The curve of M20D can be characterised by five phases: (i) a linear elasticity, (ii) a slow plasticisation up to the peak crushing force, (iii) the first abrupt load drop, (iv) a crushing force plateau, and (v) the second abrupt load drop. However, the curve of M30D just includes the first three phases. Instead of an abrupt load drop, the curves of S40S and S40D show a slow load drop at the third phase. All the phases mentioned above are associated with the different deformation and fracture modes for the different structures during the bending process which will be discussed in the next subsection.

#### 4.1.2. Quantitative comparisons

As can be seen in Table 2, the quantitative comparisons between the empty and foam-filled beams clearly reveal that the load carrying capacity of the thin-walled beams can be significantly improved by filling their cavities with PUR foam. Moreover, it is also evident the foam-filled beam with the higher foam density reaches higher load carrying capacity. This can be observed by comparing the peak crushing force of the structures. For example, S40S achieved nearly 3.2 times and 1.6 times higher peak crushing force than SES and S20S, respectively. M20D achieved nearly 5.3 times and 3.5 times higher peak crushing force than MED and M05D, respectively. On the other hand, the foam-filled beams tend to

thoroughly break into two parts, in particular for the foam-filled magnesium beams. Moreover, the comparison of the maximum deflection for the foam-filled beams indicates that the increase of the foam density leads to a decrease of the maximum deflection, which limits the EA of the foam-filled beams. The maximum deflection of the foam-filled magnesium beams is much smaller than that of the foam-filled steel beams, which indicates that the foam-filled magnesium beams are not suitable for the applications which require large deformation.

#### 4.2. Deformation and fracture modes

The deformation and fracture modes of the magnesium thin-walled beams at the beginning and final stages of three-point bending tests are shown in Figure 8. For comparison purposes, the corresponding deformation images of the steel thin-walled beams are given in Figure 9. The comparisons of these images indicate that there are some similar and dissimilar characteristics of the deformation and fracture modes between the magnesium and steel beams. The magnesium beams mainly failed by global buckling, crack propagation and fracture, however the steel beams except S40S and S40D mainly failed by global buckling, localised plastic hinges and fold formation.

##### 4.2.1. Empty and low density foam-filled beams

The empty beams, i.e. MED and SES as can be seen in Figure 8(a) and 8(b) and Figure 9(a) and 9(b), failed by global buckling in the middle just underneath the indenter at the early stage of the bending process, and accordingly the bending resistance dropped slowly at deflections of 70 mm and 25 mm, respectively, as shown in Figure 7. A large inward fold at the compression wall and two large outward folds at the adjacent side walls were developed in the case of SES. By contrast, in the

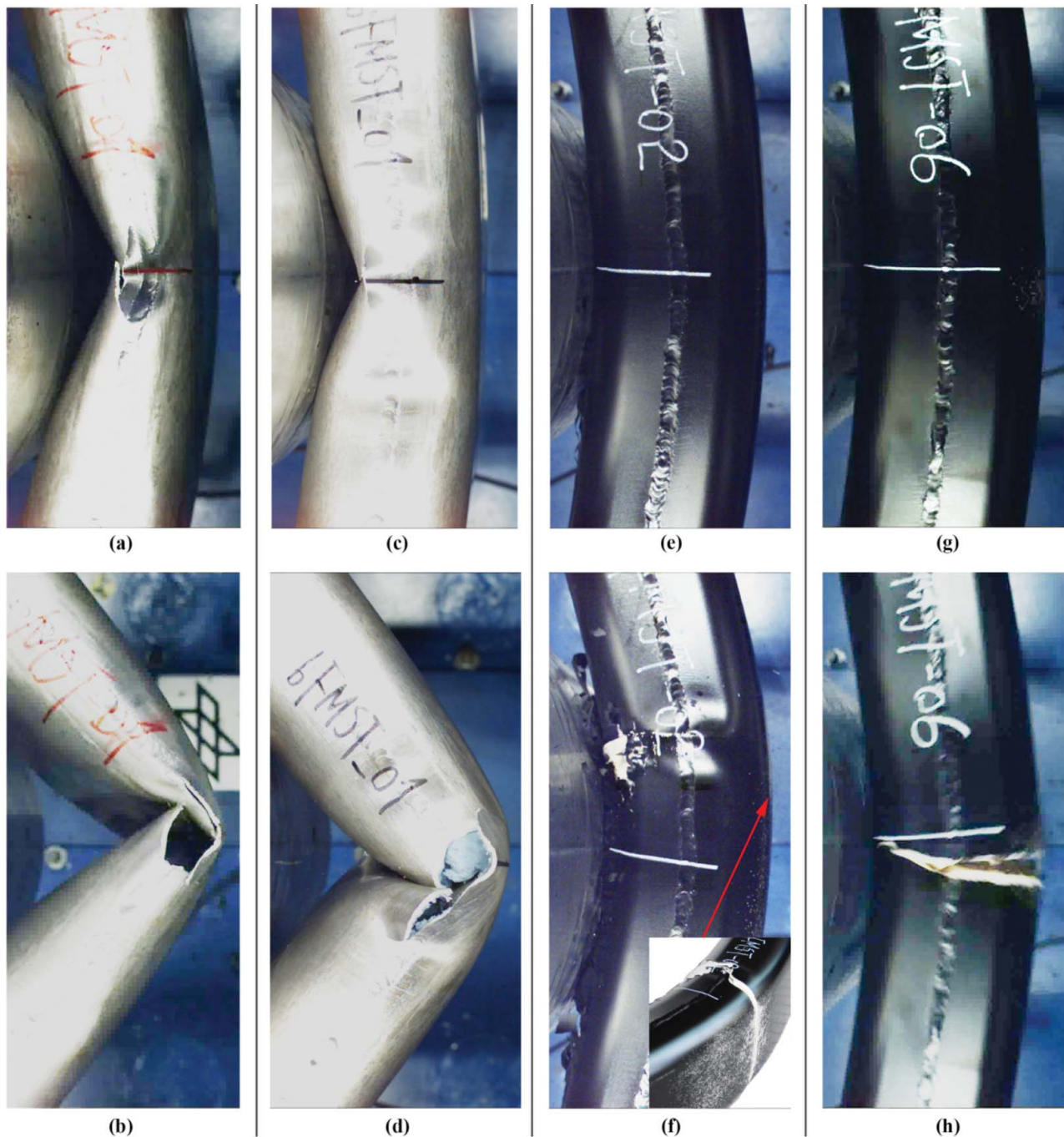


**Figure 8.** Deformation and fracture modes of the magnesium beams at the beginning and final stages of three-point bending tests: (a)–(b) MED, (c)–(d) M05D, (e)–(f) M20D and (g)–(h) M30D.

case of MED, several cracks initiated at the tip of the outward folds and propagated along the longitudinal and transverse directions of the beam. It was observed that M05D, which was filled with the  $0.05 \text{ g/cm}^3$  spray PUR pre-polymer foam, also failed by global buckling and crack propagation at the early stage of the bending process as shown in Figure 8(c) and 8(d), which indicates that the foam filler with the low foam density could not provide enough lateral support for the beam walls to

suppress the inward folding formation. Therefore, the shape of the force–deflection curve of M05D is similar to that of MED.

#### 4.2.2. Medium and high density foam-filled beams

For the foam-filled magnesium and steel beams with the medium foam density ( $0.2 \text{ g/cm}^3$ ) and high foam densities ( $0.30$  and  $0.40 \text{ g/cm}^3$ ), significant stabilisation of the cross-sections was observed during the bending process.

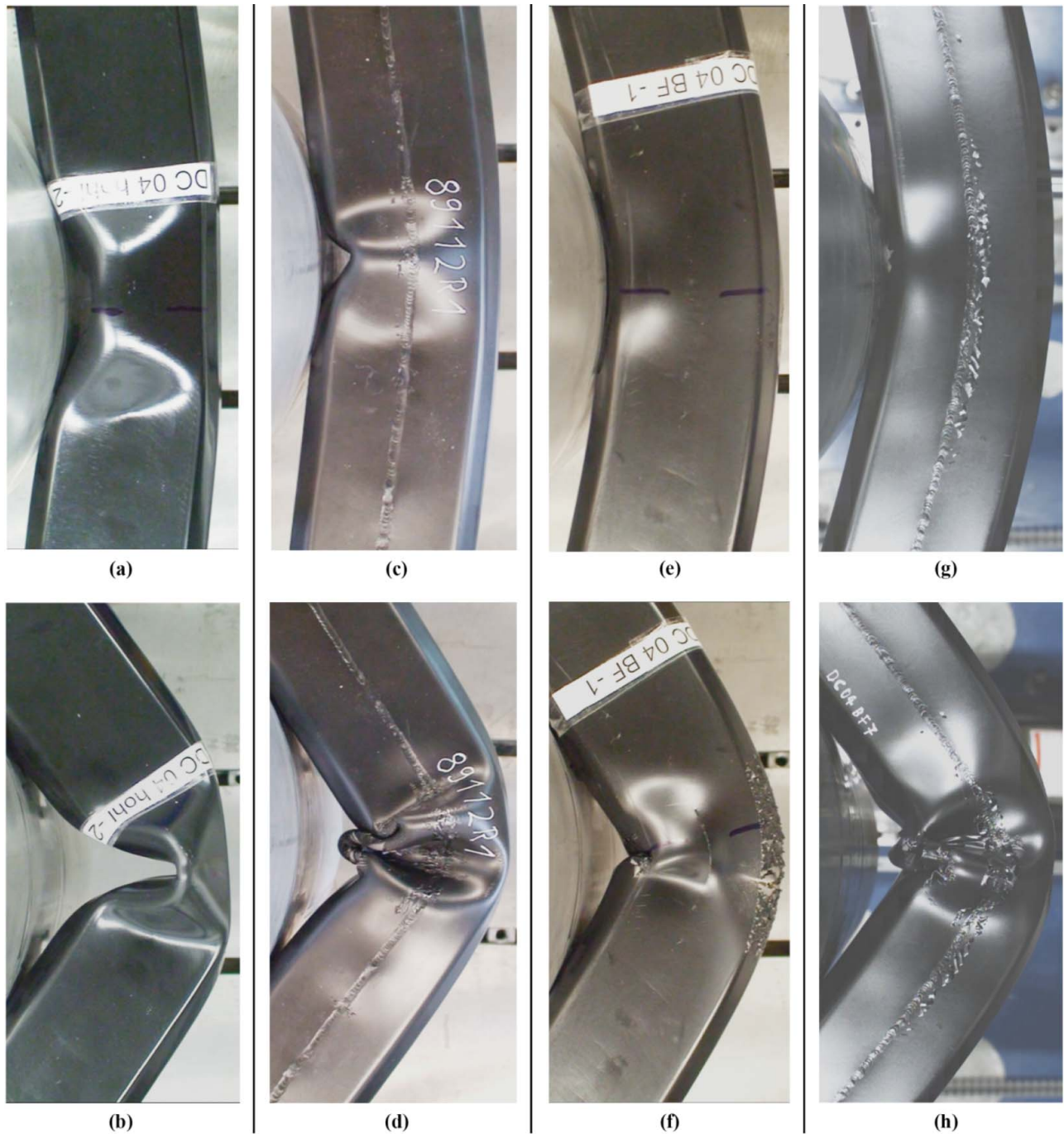


**Figure 9.** Deformation and fracture modes of the steel beams at the beginning and final stages of three-point bending tests: (a)–(b) SES, (c)–(d) S20S, (e)–(f) S40S and (g)–(h) S40D [30].

In such cases, the foam fillers retarded or even suppressed the large inward folding formations by providing sufficient lateral support for the beam walls, and accordingly the global buckling of the beam cross-sections was impeded and the plastic deformation propagated to the adjacent cross-sections, which was mirrored by the significant improvement of bending resistance and delayed load drop as can be seen in Figure 7. Moreover, there is a clear tendency showing that the higher the foam

density was, the stronger the stabilisation effect of the cross-section could be achieved. However, this stabilisation effect may result in a premature fracture at the tension side.

#### 4.2.3. Comparisons of the foam-filled beams

Different deformation and fracture modes were observed between the foam-filled magnesium and steel beams. In the case of S20S as shown in Figure 9(c) and 9(d), a small

inward fold occurred at the beginning of the bending process, leading to a slow load drop at a small deflection of about 20 mm as can be seen in Figure 7(b). In the subsequent loading stages, the foam filler inhibited the development of the inward fold and another inward fold was developed due to the jamming of the first inward fold, and therefore the bending resistance started to slowly climb up to a crushing force plateau. By contrast, M20D held almost the same rectangular shape of its cross-sections during the whole bending process and no wrinkles or plastic hinges were observed at its compression wall as shown in Figure 8(e) and 8(f). Instead, a crack abruptly occurred at the compression wall, leading to an abrupt load drop at the third phase of the force–deflection curve. This can be explained with the low ductility of the magnesium shell in compression as illustrated in Figure 5(b). The crack propagated along the transverse direction until another crack occurred at the tension wall, leading to the second abrupt load drop at the fifth phase. As shown in Figure 8(g) and 8(h), M30D exhibited a similar deformation mode to M20D; however, a crack abruptly occurred only at the tension wall instead of two cracks in M20D. Similarly, a crack occurred at the tension wall of S40S and S40D as shown in Figure 9(e)–(h), although no cracks were observed in S20S.

#### 4.2.4. Influence of corner type and welding process

The corner type of thin-walled beams may affect the fracture behaviour in some cases since large plastic deformation may localised at the corners. As shown in Figure 8(a)–(d), MED and M05D firstly fractured at the transition region between the fillets and the side walls. This may be related to the large localised plastic deformation and the stress triaxiality at this region. For M20D and M30D as shown in Figure 8(e)–(h), it seems that the filleted corners may not affect the fracture behaviour since the beams firstly fractured at the compression wall and tension wall, respectively. This fracture behaviour will be discussed in Section 5.3. For the steel beams, no fractures at the steel walls were captured in SES and S20S as shown in Figure 9(a)–(d). S40S and S40D didn't firstly fractured at the chamfered corners, but firstly fractured at the tension walls. It indicates that the chamfered corners also may not affect the fracture behaviour in such cases. In other words, substituting the filleted corners for the chamfered corners may not change the fracture behaviour of the foam-filled steel beams in the current loading and boundary conditions.

The resistance seam welding and tungsten inert gas welding processes may also affect the mechanical behaviour of thin-walled structures in some applications. The welding processes may change the material

microstructures and mechanical properties in the heat-affected zone (HAZ). The material ductility may become worst and some imperfections or initial micro-cracks may be produced in the HAZ; therefore, the structures may firstly fracture in the HAZ. In the current applications, the beams didn't firstly fracture in the HAZ, nor did the crack propagation was affected by the HAZ as shown in Figures 8 and 9. It indicates that the sheet metals were well connected by the welding processes and the welding processes didn't affect the fracture behaviour of both the magnesium and steel beams.

## 5. Discussion

This section will discuss the effects of material, strain rate, strain hardening rate and fracture behaviour on the EA capacity of the magnesium and steel beams. Possible solutions to make further improvements on the EA capacity of the tested structures will also be discussed at the end.

### 5.1. Energy absorption capacity

Two most important crashworthiness indicators including the EA and specific energy absorption (SEA) were used to evaluate the crashworthiness of the tested structures. The EA can be calculated by integrating the area under the experimental force–deflection curve. The SEA can be calculated by dividing the EA by the total mass of the structure. Table 2 summarises the EA and SEA of all the tested structures at four different deflections. To emphasise the comparison, the EA and SEA calculated at the deflection of 250 and 450 mm are shown in Figure 10.

#### 5.1.1. Steel beams

First, the results at a maximum deflection of 450 mm will be discussed. For the steel thin-walled beams, it is evident that all the foam-filled beams achieved significantly higher EA and SEA compared with the empty beam; moreover, the foam-filled beam with the high foam density of 0.4 g/cm<sup>3</sup> absorbed more energy and reached higher SEA than that filled with the medium foam density of 0.2 g/cm<sup>3</sup>. The effect of strain rate on EA capacity was observed for the foam-filled steel beams. S40D achieved nearly 7% higher EA than S40S, which seems to indicate that the strain rate effect on the EA was not significant in the current structures and loading conditions.

#### 5.1.2. Magnesium beams

However, the results from the magnesium thin-walled beams indicate that the foam density has a complex

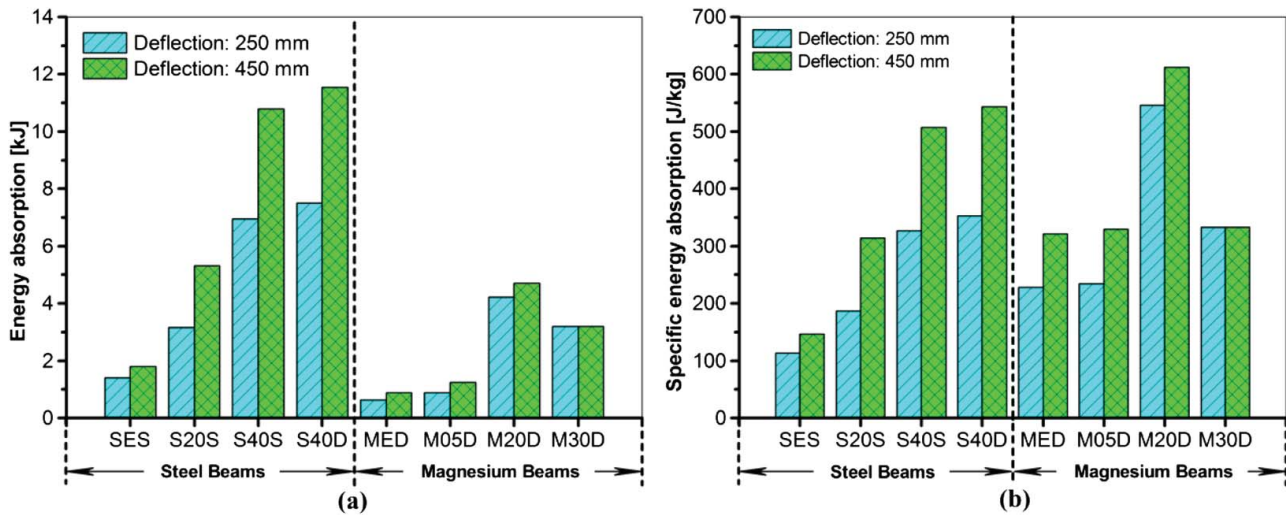


**Figure 10.** Energy absorption capacity of different tested structures at the deflection of 250 mm and 450 mm: (a) energy absorption and (b) specific energy absorption.

relationship with the EA and SEA. For example, M20D achieved 5.4 times higher EA than MED, while the mass itself increased by a factor of 2.8, and consequently M20D reached an increase of the SEA by a factor of nearly 1.9 times. By contrast, M05D and M30D achieved 1.4 times and 3.6 times higher EA than MED, but the corresponding SEA values were almost identical to that of MED because the mass itself increased simultaneously by an almost identical factor. Notably, M30D exhibited moderately higher load carrying capacity than M20D, but it was thoroughly broken up into two pieces at a considerably smaller deflection, and consequently M30D absorbed even lower energy than M20D. It may imply that the SEA of the foam-filled magnesium beams has a nonlinear non-monotonic relationship with the foam density in the range of 0.05–0.3 g/cm<sup>3</sup>. This relationship seems to be still valid when the SEA is calculated at a smaller deflection.

### 5.1.3. Comparisons between the steel and magnesium beams

As listed in Table 1, the magnesium beams were tested at a testing speed of 2.0 or 3.5 m/s. At this speed level, the maximum average strain rate at the bending region of the beams should be less than 1/s. In such conditions, the effect of strain rate on load carrying capacity should be relatively slight or moderate [49]. Moreover, the difference of the mechanical responses between the steel and magnesium structures is significant. Therefore, quantitative comparisons of the EA and SEA between the steel and magnesium beams would make sense. For example, MED achieved much higher SEA than SES, which indicates that magnesium alloy AZ31B may potentially outperform steel DC04 in terms of the SEA

for empty thin-walled beams when subjected to bending loads. With a foam density of 0.20 g/cm<sup>3</sup>, M20D reached much higher SEA than S20S within a deflection of 450 mm. On the other hand, M20D reached nearly 13% higher SEA than S40D; however, this outperformance in terms of SEA is limited because the foam-filled magnesium beams tend to prematurely fracture and subsequently M20D absorbed much less energy than S40D.

The EA and SEA at smaller deflections than 450 mm are summarised in Table 2. M20D reached nearly 31%, 55% and 47% higher SEA than S40D at 350, 250 and 150 mm deflections, respectively, which indicates that the outperformance in terms of the SEA for foam-filled magnesium beams becomes significant at a smaller deflection. In particular, M20D obtained nearly 33% higher EA and 2.9 times higher SEA than S20S at a deflection of 250 mm, although M20D was nearly 54% lighter than S20S and even 38% lighter than SES. Even at a deflection of 350 mm, M20D obtained nearly 9% higher EA and 2.4 times higher SEA than S20S. In many real-world passenger car side impact scenarios, the intrusion displacement of relevant components is limited to a smaller range due to space protection constraints. For example, the intrusion displacement of rocker rails in passenger cars is generally limited to about 250 mm to protect passenger safety. These structures together with the surrounding components such as B-pillars, door panels and floor beams absorb sufficient energy. It suggests that there are possibilities to develop lighter auto-body structures such as rocker rails by substituting magnesium alloy AZ31B for steel DC04, while maintaining or exceeding their current crashworthiness and safety.

## 5.2. Effect of strain hardening rate

As discussed in the previous section, the outperformance of the foam-filled magnesium beams is associated with the deformation modes under three-point bending loads. Our previously published study [30] suggests that generally the inward fold occurs earlier during the bending process, if the strength of the metallic shell is increased in relation to the compressive strength of the foam filler. At a larger wall thickness, the ability of the foam filler to prevent the buckling of the compression wall is reduced, which leads to a decrease of SEA in combination with a higher mass itself. On the other hand, it was observed that more material in M20D was involved in plastic deformation compared with that in the foam-filled steel beams. As illustrated in Figure 11, three points marked at the side walls of the foam-filled beams were used to roughly measure the bending angle  $\theta$  before the inward fold occurred during the bending process. It can be assumed that more material is involved at the plastic bending region if the bending angle  $\theta$  is larger. Figure 11 (b)–(d) sketches a comparison of the bending angle  $\theta$  between the foam-filled magnesium and steel beams. M20D obtained a larger bending angle than S20S, S40S and S40D. This is probably due to the high work hardening rate of AZ31B sheet in compression. The work hardening with higher rate spread the plastic deformation over more material causing the foam-filled magnesium

beams to deform with a larger radius of curvature than the foam-filled steel beams. This is an important factor which may result in more energy to be absorbed for the foam-filled magnesium beams in bending compared with the foam-filled steel beams. Similar observations were reported by other researchers [19,27].

## 5.3. Macro-fracture analysis

### 5.3.1. Fracture behaviour of the PUR foams

The stabilisation effect of the cross-section by foam filling increased the tensile stress at the tension side of the foam filler. Thus, several cracks initiated and propagated along the transverse direction within the foam filler as can be seen in Figure 12, which can be explained with the brittle fracture behaviour of the PUR foams in



Figure 12. Sectional view of the foam-filled steel beam S40S in three-point bending tests [30].

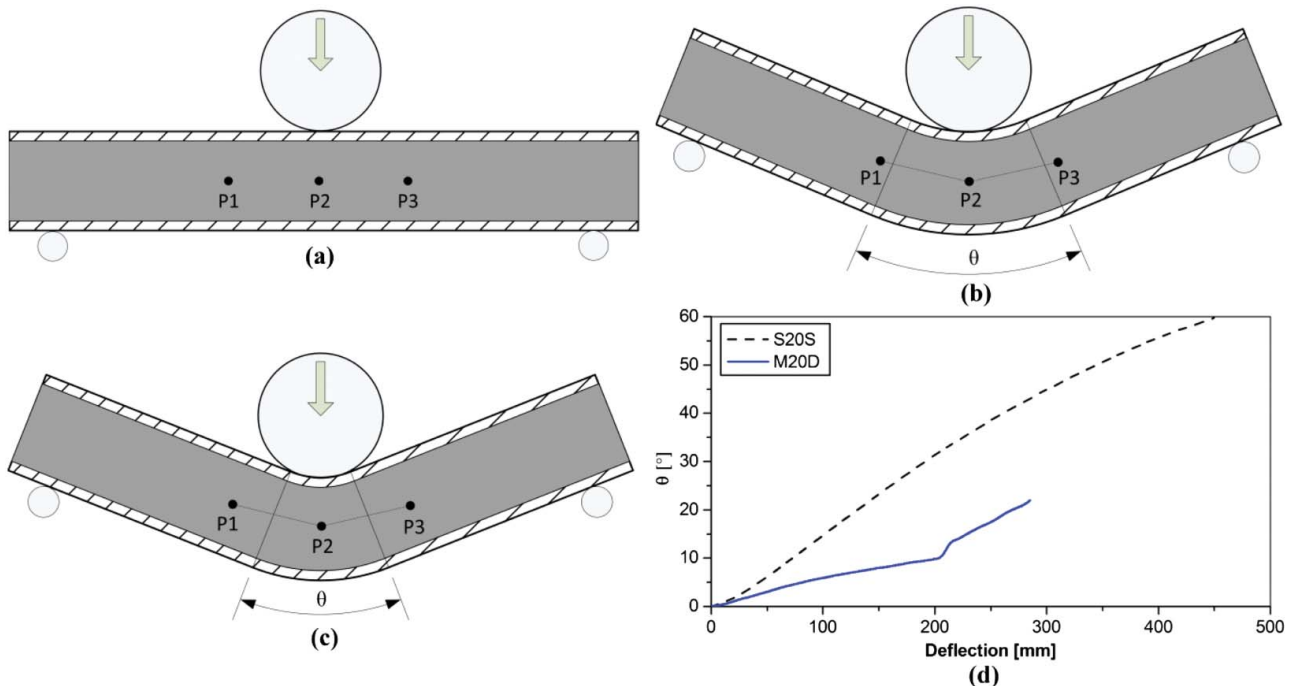


Figure 11. Schematic of deformation modes for foam-filled magnesium and steel beams: (a) initial position, (b) foam-filled magnesium beam, (c) foam-filled steel beam and (d) evolution of bending angle with respect to deflection. The symbol  $\theta$  represents the bending angle. The symbols P1, P2, P3 represent the three points marked at the side walls of the foam-filled beams and their displacements were captured during the bending process.

tension as illustrated in Figure 5(c). The cell-edge alignment and stretching dominate the deformation mechanisms of the PUR foams under tensile stress, while the cell-edge buckling and folding dominate the deformation mechanisms under compressive stress. This is an inherent characteristic of the PUR foams, where the material exhibits brittle behaviour in tension and much more ductile behaviour in compression. During the propagation of the foam cracks, the stretching deformation of the metallic shell was localised in the vicinity of these foam cracks, leading to a subsequent crack at the weakest point of the tension wall.

### 5.3.2. Fracture behaviour of the magnesium shells

The premature fracture is a critical issue in the EA capacity of the foam-filled magnesium beams due to the inferior ductility of AZ31B sheet at room temperature. As illustrated in Figures 7 and 8, the fracture behaviour of the shell materials, especially in the foam-filled magnesium beams with foam densities of 0.20 and 0.30 g/cm<sup>3</sup>, was found to be a major limitation to their energy absorption. In order to analyse the fracture behaviour of the magnesium shells at a macro-level, the longitudinal elongation at the tension walls of M20D and M30D was measured by strain gauges during the three-point bending tests. The measured maximum elongation near the cracks is about 7%, which is close to the effective failure strain measured in the plane strain condition as illustrated in Figure 6. It can be explained by the fact that the deformation at the tension walls is in a quasi-plane strain condition because the foam fillers confined the transverse contraction of the magnesium shells at the tension walls of M20D and M30D. In other words, the inferior ductility of AZ31B sheet at room temperature is an inherent reason which caused the premature fracture of the foam-filled magnesium beams; moreover, the foam fillers confined the transverse contraction of the magnesium shells at the tension walls of M20D and M30D and subsequently aggravated the premature fracture.

### 5.4. Possibilities of further improvements

In Section 5.1.3, the experimental results show that the foam-filled magnesium beam significantly outperforms the foam-filled steel beam when the beams were filled with 0.20 g/cm<sup>3</sup> foam and the deflection was limited to less than 350 mm. It should be possible, therefore, to develop lightweight auto-body structures such as rocker rails by substituting AZ31B for DC04, because the intrusion displacement of such structures in passenger cars is generally limited to about 250 mm to protect passenger

safety according to most passive safety regulations and NCAP side impact tests.

However, further improvements will be made to overcome the issue of the premature fracture at the tension wall of the foam-filled magnesium beam, because the premature fracture could significantly reduce the passive safety when a passenger car is subjected to more severe crash accidents. The possibilities of further improvements include:

- (1) Improve the ductility of AZ31B sheet by using new manufacturing processes.
- (2) Develop new magnesium alloys with higher ductility, such as magnesium-rare earth alloys ZE10 [41] and ZEK100 [31].
- (3) Substitute steels or aluminium alloys with higher ductility for AZ31B sheet at the tension wall if suitable joining and corrosion protection methods are developed.
- (4) Make the AZ31B shell at the tension wall to deform at a stress state which is close to the uniaxial tension condition by optimising the foam density and its distribution in the cavity of the beam.

On the other hand, the current experimental study observed that the SEA of the foam-filled magnesium beams has a nonlinear non-monotonic relationship with the foam density. Therefore, future work will focus on to find a foam density that should be used to achieve an optimal SEA.

The numerical simulation study conducted by two of current authors [30] indicates that the wall thickness has a significant effect on the mechanical properties of foam-filled beams. Furthermore, the mechanical properties of the AZ31B beams under three-point bending loads may also be affected by the manufacturing processes, such as the effect of cold bending induced pre-strain on the stress–strain response of AZ31B sheet, the effect of tungsten inert gas welding on the material microstructures and mechanical properties in the heat affected zone, and the effect of cathodic dip painting on the interface bonding between the metallic shell and foam filler. These topics are interesting and worthwhile to study in the future.

## 6. Conclusions

This study has proposed a hybrid structural design concept of the PUR foam-filled AZ31B beams which serves as energy absorbing components in automotive applications. The uniaxial tensile and compressive tests, fracture tests and dynamic three-point bending tests on magnesium alloy AZ31B sheet and rectangular thin-walled

beams filled with PUR foams has been performed. The main conclusions of this study are listed as follows:

- (1) The strengthening effect of PUR foam filling on AZ31B rectangular thin-walled beams has been observed. It suggests that the foam-filled AZ31B beam with a higher foam density achieves higher load carrying capacity, but fractures at a smaller deflection.
- (2) The foam-filled AZ31B beam can absorb more energy and reaches higher specific EA than the foam-filled steel DC04 beam, while achieving an even lighter structure than the empty steel DC04 beam, when the beams were filled with  $0.20 \text{ g/cm}^3$  foam and the deflection was limited to less than 350 mm.
- (3) The foam-filled AZ31B beams outperformed the foam-filled DC04 beams in specific energy absorption, although neither structure has been optimised via a combination of foam density and wall thickness.
- (4) The potential advantage of the foam-filled AZ31B beams in EA is possibly associated with the high work hardening rate of AZ31B sheet in compression, which may involve more material in the plastic deformation compared with the foam-filled DC04 beams.
- (5) Therefore, the hybrid structural design concept of the PUR foam-filled AZ31B beams has potential applications in auto-body structures such as rocker rails.

However, the foam-filled magnesium beams have significantly lower total EA when high-density foam is used, because the foam-filled AZ31B beams tend to prematurely fracture at the compression and tension walls. Therefore, further improvements will be made to overcome the issue of the premature fracture, because the premature fracture could significantly reduce the passive safety when a passenger car is subjected to more severe crash accidents.

## Acknowledgements

The authors thank Philipp Strassburger, Cedric Rieger and Thomas Grünheid (DLR-Institute of Vehicle Concepts) for their kind assistance in conducting the component three-point bending tests. The authors also thank Martin Holzapfel and Harald Kraft (DLR-Institute of Structures and Design) for their kind assistance in material coupon tests. The authors wish to acknowledge Katja Oswald and Jan Roettger (The Dow Chemical Company), who provided the BETAFOAM™ PUR foam filling for the PUR foams.

## Disclosure statement

No potential conflict of interest was reported by the authors.

## Funding

This work is supported by the DLR project 'Next Generation Car'.

## ORCID

Ping Zhou  <http://orcid.org/0000-0002-1024-1209>

## References

- [1] U. Ali, *Numerical modeling of failure in magnesium alloys under axial compression and bending for crashworthiness applications*, Master thesis, University of Waterloo, 2012.
- [2] R.A. Arbelaez, *Side Impact Challenges for Steel Vehicle Structures*, Insurance Institute for Highway Safety, 2005. Available at <http://www.steel.org>
- [3] M. Avalle, G. Belingardi, and R. Montanini, *Characterization of polymeric structural foams under compressive impact loading by means of energy-absorption diagram*, *Int. J. Impact Eng.* 25 (2001), pp. 455–472.
- [4] Y. Bao and T. Wierzbicki, *On fracture locus in the equivalent strain and stress triaxiality space*, *Int. J. Mech. Sci.* 46 (2004), pp. 81–98.
- [5] E. Beeh, P. Zhou, P. Straßburger, H.E. Friedrich, R. Smith, W. Altenhof, and M. Worswick, *Novel Concepts to Apply Magnesium in Crash-Related Vehicle Structures*, IMA's 72nd Annual World Magnesium Conference, Vancouver, Canada, 2015.
- [6] P.D. Beggs, W. Song, and M. Easton, *Failure modes during uniaxial deformation of magnesium alloy AZ31B tubes*, *Int. J. Mech. Sci.* 52 (2010), pp. 1634–1645.
- [7] W. Chen, *Experimental and numerical study on bending collapse of aluminum foam-filled hat profiles*, *Int. J. Solids Struct.* 38 (2001), pp. 7919–7944.
- [8] W. Chen, F. Lu, and N. Winfree, *High-strain-rate compressive behavior of a rigid polyurethane foam with various densities*, *Exp. Mech.* 42 (2002), pp. 65–73.
- [9] C. Dørum, O.S. Hopperstad, O.G. Lademo, and M. Langseth, *Aluminium and magnesium castings – experimental work and numerical analyses*, *Int. J. Crashworthiness* 8 (2003), pp. 455–470.
- [10] C. Dørum, O.S. Hopperstad, O.G. Lademo, and M. Langseth, *Numerical modelling of the structural behaviour of thin-walled cast magnesium components*, *Int. J. Solids Struct.* 42 (2005), pp. 2129–2144.
- [11] C. Dørum, O.S. Hopperstad, O.-G. Lademo, and M. Langseth, *Energy absorption capacity for thin-walled AM60 castings using a shear-bolt principle*, *Comput. Struct.* 85 (2007), pp. 89–101.
- [12] C. Dørum, O. Sture Hopperstad, O.-G. Lademo, and M. Langseth, *An experimental study on the energy absorption capacity of thin-walled castings*, *Int. J. Impact Eng.* 32 (2006), pp. 702–724.
- [13] A. Droste, O. Bijjargi, D. Wang, and B. Qi, *Potentials of Polymeric-Based Body Structural Materials in Full Car Crash*, LS-DYNA Update Forum, Filderstadt, 2009.



- [14] I. Duarte, M. Vesenjajk, and L. Krstulović-Opara, *Dynamic and quasi-static bending behaviour of thin-walled aluminium tubes filled with aluminium foam*, *Compos. Struct.* 109 (2014), pp. 48–56.
- [15] I. Duarte, M. Vesenjajk, L. Krstulović-Opara, I. Anžel, and J.M.F. Ferreira, *Manufacturing and bending behaviour of in situ foam-filled aluminium alloy tubes*, *Mater. Design* 66 (2015), pp. 532–544.
- [16] M. Dunand and D. Mohr, *On the predictive capabilities of the shear modified Gurson and the modified Mohr–Coulomb fracture models over a wide range of stress triaxialities and Lode angles*, *J. Mech. Phys. Solids* 59 (2011), pp. 1374–1394.
- [17] M. Easton, A. Beer, M. Barnett, C. Davies, G. Dunlop, Y. Durandet, S. Blacket, T. Hilditch, and P. Beggs, *Magnesium alloy applications in automotive structures*, *JOM J. Min. Met. Mat. S.* 60 (2008), pp. 57–62.
- [18] M. Easton, M. Gibson, A. Beer, M. Barnett, C. Davies, Y. Durandet, S. Blacket, X. Chen, N. Birbilis, and T. Abbott, *Sustainable automotive technologies 2012*, A. Subic, J. Wellnitz, M. Leary, and L. Koopmans, eds., 2012. doi: 10.1007/978-3-642-24145-1\_3
- [19] M. Easton, W. Qian Song, and T. Abbott, *A comparison of the deformation of magnesium alloys with aluminium and steel in tension, bending and buckling*, *Mater. Design* 27 (2006), pp. 935–946.
- [20] J.H. Forsmark, M. Li, X. Su, D.A. Wagner, J. Zindel, A.A. Luo, J.F. Quinn, R. Verma, Y.-M. Wang, S.D. Logan, S. Bilkhu, and R.C. McCune, *The USAMP Magnesium Front End Research and Development Project – Results of the Magnesium “Demonstration” Structure*, *Magnesium Technology 2014*, John Wiley & Son, Hoboken, NJ, 2014, pp. 517–524.
- [21] H.E. Friedrich and B.L. Mordike, *Magnesium Technology – Metallurgy, Design Data, Applications*, Springer-Verlag, Heidelberg, 2006.
- [22] D. Ghaffari Tari, M.J. Worswick, U. Ali, and M.A. Gharghouri, *Mechanical response of AZ31B magnesium alloy: Experimental characterization and material modeling considering proportional loading at room temperature*, *Int. J. Plast.* 55 (2014), pp. 247–267.
- [23] L.J. Gibson and M.F. Ashby, *Cellular Solids: Structure and Properties*, Pergamon Press, Oxford, 1997.
- [24] M. Goede, M. Stehlin, L. Rafflenbeul, G. Kopp, and E. Beeh, *Super light car—lightweight construction thanks to a multi-material design and function integration*, *Eur. Transport Res. Rev.* 1 (2008), pp. 5–10.
- [25] G. Gruben, E. Fagerholt, O.S. Hopperstad, and T. Børvik, *Fracture characteristics of a cold-rolled dual-phase steel*, *Eur. J. Mech. A. Solids* 30 (2011), pp. 204–218.
- [26] A.G. Hanssen, O.S. Hopperstad, and M. Langseth, *Bending of square aluminium extrusions with aluminium foam filler*, *Acta Mech.* 142 (2000), pp. 13–31.
- [27] T. Hilditch, D. Atwell, M. Easton, and M. Barnett, *Performance of wrought aluminium and magnesium alloy tubes in three-point bending*, *Mater. Design* 30 (2009), pp. 2316–2322.
- [28] K.Y. Jeong, S.S. Cheon, and M.B. Munshi, *A constitutive model for polyurethane foam with strain rate sensitivity*, *J. Mech. Sci. Technol.* 26 (2012), pp. 2033–2038.
- [29] P.E. Krajewski, A. Ben-Artzy, and R.K. Mishra, *Room Temperature Tensile Anisotropy of Extruded Magnesium Plates*, *Magnesium Technology 2010*, TMS (The Minerals, Metals & Materials Society), John Wiley & Sons, Hoboken, NJ, 2010, pp. 467–472.
- [30] M. Kriescher, W. Salameh, E. Beeh, J. Roettger, A. Droste, and M. Otto, *Possibilities for the Use of Metal-Hybrid-Structures for Vehicle Crash Load Cases*, *Euro Hybrid Materials and Structures*, Private University of Applied Sciences, Stade, 2014, pp. 115–120.
- [31] S. Kurukuri, M.J. Worswick, A. Bardelcik, R.K. Mishra, and J.T. Carter, *Constitutive behavior of commercial grade ZEK100 magnesium alloy sheet over a wide range of strain rates*, *Metall. Mater. Trans. A* 45 (2014), pp. 3321–3337.
- [32] S. Kurukuri, M.J. Worswick, D. Ghaffari Tari, R.K. Mishra, and J.T. Carter, *Rate sensitivity and tension-compression asymmetry in AZ31B magnesium alloy sheet*, *Philos. Trans. A Math. Phys. Eng. Sci.* 372 (2014) pp. 20130216–20130216.
- [33] X.Z. Lin and D.L. Chen, *Strain hardening and strain-rate sensitivity of an extruded magnesium alloy*, *J. Mater. Eng. Perform.* 17 (2008), pp. 894–901.
- [34] X. Lou, M. Li, R. Boger, S. Agnew, and R. Wagoner, *Hardening evolution of AZ31B Mg sheet*, *Int. J. Plast.* 23 (2007), pp. 44–86.
- [35] N.-T. Nguyen, O. Seo, C. Lee, M.-G. Lee, J.-h. Kim, and H. Kim, *Mechanical behavior of AZ31B Mg alloy sheets under monotonic and cyclic loadings at room and moderately elevated temperatures*, *Materials* 7 (2014), pp. 1271–1295.
- [36] M. Paulino and F. Teixeira-Dias, *On the use of polyurethane foam paddings to improve passive safety in crash-worthiness applications, in Polyurethane*, F. Zafar and E. Sharmin, eds., InTech, Rijeka, Croatia, 2012.
- [37] J. Rossiter, K. Inal, and R. Mishra, *Numerical modeling of the failure of magnesium tubes under compressive loading*, *J. Eng. Mater. Technol.* 134 (2012), pp. 021008.
- [38] J. Rossiter, K.A. Inal, and R.K. Mishra, *Numerical Modeling of Failure in Magnesium Alloys During Crush Simulations*, *Magnesium Technology 2010*, TMS (The Minerals, Metals & Materials Society), John Wiley & Sons, Hoboken, NJ, 2010, pp. 293–296.
- [39] S. Santosa, J. Banhart, and T. Wierzbicki, *Bending Crush Behavior of Foam-Filled Sections*, *Metal Foams and Porous Metal Structures*, MIT Verlag, Bremen, 1999, pp. 337–345.
- [40] S. Santosa and T. Wierzbicki, *Effect of an ultralight metal filler on the bending collapse behavior of thin-walled prismatic columns*, *Int. J. Mech. Sci.* 41 (1999), pp. 995–1019.
- [41] D. Steglich, X. Tian, J. Bohlen, S. Riekehr, N. Kashaev, K. U. Kainer, and N. Huber, *Experimental and numerical crushing analyses of thin-walled magnesium profiles*, *Int. J. Crashworthiness* 20 (2015), pp. 177–190.
- [42] I. Ulacia, C.P. Salisbury, I. Hurtado, and M.J. Worswick, *Tensile characterization and constitutive modeling of AZ31B magnesium alloy sheet over wide range of strain rates and temperatures*, *J. Mater. Process. Technol.* 211 (2011), pp. 830–839.
- [43] D.A. Wagner, S. Logan, K. Wang, T. Skszek, and C.P. Salisbury, *Test Results and FEA Predictions from Magnesium AM30 Extruded Beams in Bending and Axial Compression*, *Magnesium Technology 2009*, The Minerals,

- Metals and Materials Society, John Wiley & Sons, Hoboken, NJ, 2009, pp. 541–549.
- [44] D.A. Wagner, S.D. Logan, K. Wang, and T. Skszek, *Test Results and FEA Predictions from Magnesium AZ31 Sheet Beams in Bending and Axial Compression*, Magnesium Technology 2010, TMS (The Minerals, Metals & Materials Society), John Wiley & Sons, Hoboken, NJ, 2010, pp. 547–552.
- [45] T. Wierzbicki, Y. Bao, Y.-W. Lee, and Y. Bai, *Calibration and evaluation of seven fracture models*, Int. J. Mech. Sci. 47 (2005), pp. 719–743.
- [46] S. Xu, W.R. Tyson, R. Eagleson, R. Zavadil, Z. Liu, P.L. Mao, C.Y. Wang, S.I. Hill, and A.A. Luo, *Dependence of flow strength and deformation mechanisms in common wrought and die cast magnesium alloys on orientation, strain rate and temperature*, J. Magnesium Alloys 1 (2013), pp. 275–282.
- [47] H.R. Zarei and M. Kröger, *Bending behavior of empty and foam-filled beams: Structural optimization*, Int. J. Impact Eng. 35 (2008), pp. 521–529.
- [48] P. Zhou, E. Beeh, and H.E. Friedrich, *A novel testing method for uniaxial compression of thin-sheet magnesium alloys*, Exp. Mech. 56 (2016), pp. 513–519.
- [49] P. Zhou, E. Beeh, H.E. Friedrich, M. Kriescher, P. Straßburger, M. Holzapfel, H. Kraft, C. Rieger, K. Oswald, and J. Roettger, *Bending collapse behaviour of polyurethane foam-filled rectangular magnesium alloy AZ31B tubes*, Mater. Sci. Forum 828–829 (2015), pp. 259–264.